

Insights into exfoliation possibility of MAX phases to MXenes

Mohammad Khazaei,^{1,*} Ahmad Ranjbar,¹ Keivan Esfarjani,²
Dimitri Bogdanovski,³ Richard Dronskowski,³ and Seiji Yunoki^{1,4,5}

¹*Computational Materials Science Research Team,
RIKEN Advanced Institute for Computational Science (AICS), Kobe, Hyogo 650-0047, Japan*

²*Department of Mechanical and Aerospace Engineering,*

University of Virginia, 122 Engineer's Way, Charlottesville, VA 22904, USA

³*Chair of Solid State and Quantum Chemistry, RWTH Aachen University, 52056 Aachen, Germany*

⁴*Computational Condensed Matter Physics Laboratory, RIKEN, Wako, Saitama 351-0198, Japan*

⁵*Computational Quantum Matter Research Team,*

RIKEN Center for Emergent Matter Science (CEMS), Wako, Saitama 351-0198, Japan

(Dated: March 15, 2018)

Chemical exfoliation of MAX phases into two-dimensional (2D) MXenes can be considered as a major breakthrough in the synthesis of novel 2D systems. To gain insight into the exfoliation possibility of MAX phases and to identify which MAX phases are promising candidates for successful exfoliation into 2D MXenes, we perform extensive electronic structure and phonon calculations, and determine the force constants, bond strengths, and static exfoliation energies of MAX phases to MXenes for 82 different experimentally synthesized crystalline MAX phases. Our results show a clear correlation between the force constants and the bond strengths. As the total force constant of an “A” atom contributed from the neighboring atoms is smaller, the exfoliation energy becomes smaller, thus making exfoliation easier. We propose 37 MAX phases for successful exfoliation into 2D Ti_2C , Ti_3C_2 , Ti_4C_3 , Ti_5C_4 , Ti_2N , Zr_2C , Hf_2C , V_2C , V_3C_2 , V_4C_3 , Nb_2C , Nb_5C_4 , Ta_2C , Ta_5C_4 , Cr_2C , Cr_2N , and Mo_2C MXenes. In addition, we explore the effect of charge injection on MAX phases. We find that the injected charges, both electrons and holes, are mainly received by the transition metals. This is due to the electronic property of MAX phases that the states near the Fermi energy are mainly dominated by d orbitals of the transition metals. For negatively charged MAX phases, the electrons injected cause swelling of the structure and elongation of the bond distances along the c axis, which hence weakens the binding. For positively charged MAX phases, on the other hand, the bonds become shorter and stronger. Therefore, we predict that the electron injection by electrochemistry or gating techniques can significantly facilitate the exfoliation possibility of MAX phases to 2D MXenes.

PACS numbers:

I. INTRODUCTION

MAX phases are a large family of solid layered transition metal carbides or nitrides with a hexagonal lattice (space group $P6_3/mmc$) and the chemical formula of $M_{n+1}AX_n$, where “M” stands for an early transition metal (Sc, Ti, Zr, Hf, V, Nb, Ta, Cr, or Mo), “A” represents an element from main groups III–VI of the periodic table (Al, Ga, In, Tl, Si, Ge, Sn, Pb, P, As, Bi, S, or Te), “X” is carbon or nitrogen, and $n = 1–4$.^[1–5] Recently, the family of crystalline MAX phases has been expanded even further. For example, a set of ordered double transition metals MAX phases of $M_2M'AX_2$, $M_2M'_2AX_3$,^[6, 7] and $(M_{2/3}M'_{1/3})_2AX_2$ has been synthesized,^[8, 9] where “M” is another transition metal. The crystal structures of MAX phases with varying stoichiometry are shown schematically in Fig. 1. To the best of our knowledge, 82 different crystalline MAX phases have been experimentally fabricated [1, 3] as listed in Table 1S. In addition to the crystalline MAX phases, various alloys of

MAX phases with different mixtures of transition metals and/or X elements have also been synthesized. Theoretically, thousands of crystalline or alloy structures of MAX phases have been predicted to be stable.^[10–20]

All MAX phases are metallic [13, 14, 21–25] because of the existence of partially occupied d orbitals of transition metals near the Fermi energy.^[13, 14] In other words, due to the metallic bonding between the transition metal atoms either on the same layer or across layers, MAX phases become electrically conductive. Since MAX phases are made of metal and nonmetal elements and are synthesized at high temperatures, they are usually considered as ceramics. Owing to their high mechanical and thermal stability,^[10, 13–15, 26, 27] some of the MAX phases could be used in harsh conditions, *i.e.*, in conditions where the materials should be resistant to thermal shock, fatigue, creep, oxidation, or corrosive reactions.^[1, 2] To enhance the technological applications of MAX phases, the ductility of MAX phases can be improved by lowering their ceramic brittleness without harming their toughness when the number of valence electrons per unit cell is properly controlled by mixing different M, A, or X elements.^[10, 13]

Up to a few years ago, the application of MAX

*Electronic address: khazaei@riken.jp

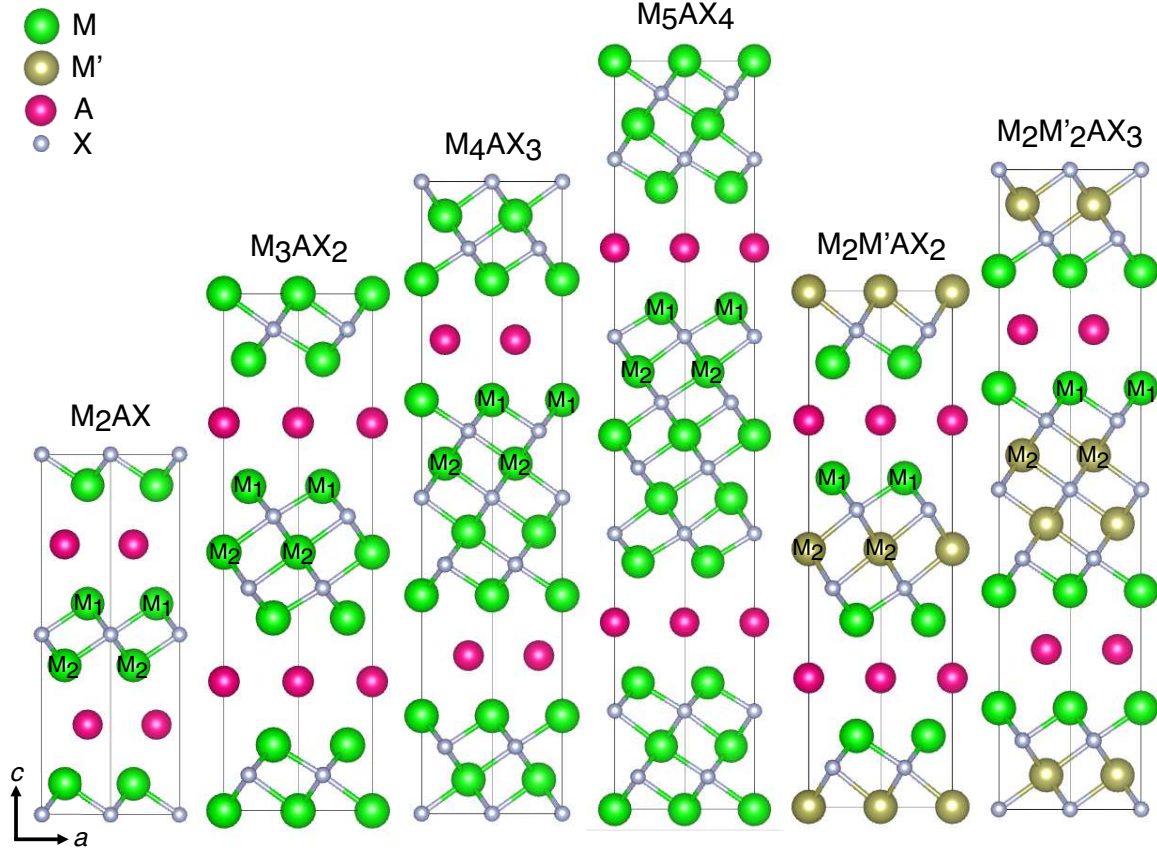


FIG. 1: Atomic structures of six different crystalline MAX phases. The a and c axes are common to all structures. Transition metals in different layers are indicated by “ M_1 ” and “ M_2 ” to denote different bonds between transition metals located in the same layer (M_1-M_1 or M_2-M_2) and in different layers (M_1-M_2). In $M_{n+1}AX_n$ ($n = 1 - 4$), M_1 and M_2 are the same type of transition metal, while they are different types in $M_2M'AX_2$ and $M_2M'_2AX_3$.

phases was based solely on their interesting mechanical properties, rather than their electronic, magnetic, or optical ones. However, the possibility of exfoliation from MAX phases into two-dimensional (2D) transition metal carbides or nitrides, so called MXenes, has significantly broadened the range of potential applications of MAX phases.[28, 29] It has been repeatedly proven experimentally that by using the combination of acid treatment and sonication, the M–A bonds in some of the MAX phases can be broken while the M–X bonds are kept almost intact. After the exfoliation process, the A atoms are washed out from the MAX phase and the remaining set of single or multilayers is MXene. The crystal structures of derived 2D MXenes, M_2X , M_3X_2 , M_4X_3 , M_5X_4 , $M_2M'X_2$, and $M_2M'_2X_3$, are shown schematically in Fig. 2. So far, the single or multilayer 2D structures of Ti_2C ,[29] Ti_2N ,[30] V_2C ,[31] Nb_2C ,[31] Mo_2C ,[32] Ti_3C_2 ,[28] Zr_3C_2 ,[33] Nb_4C_3 ,[34] Ta_4C_3 ,[29] and Ti_4N_3 [36] as well as $TiNbC$,[29] $(Ti_{0.5}Nb_{0.5})_2C$,[29] $(V_{0.5}Cr_{0.5})_3C_2$,[29] Ti_3CN ,[29] Mo_2TiC_2 ,[37] Mo_2ScC_2 ,[7] Cr_2TiC_2 ,[37] $Mo_2Ti_2C_3$,[37] $(Nb_{0.8}Ti_{0.2})_4C_3$,[35] and $(Nb_{0.8}Zr_{0.2})_4C_3$ [35] have already been synthesized. The electronic properties of

these 2D MXenes are different from their corresponding MAX phases. It is also shown theoretically that upon a particular surface functionalization, some of the MXenes turn into semiconductors.[38] In contrast to the limited application of MAX phases as structural materials, many interesting electronic,[38–44] optical,[45] mechanical,[46] magnetic,[38, 47–51] and thermoelectric [38, 39], photocatalytic [52] and many other applications [53, 54] have been theoretically proposed for 2D MXenes. Experimentally, MXenes have attracted a lot of attention in the materials science community for electronic transport,[55–57] energy storage,[58, 59] energy conversion,[60–63] and development of novel hybrid nanocomposites.[64, 65] There are comprehensive reviews on the synthesis and application,[66] and the current theoretical status [67] of MXenes in the literature.

It is now well accepted that the MAX phases are a great source for producing novel 2D systems. Considering the compositional varieties of MAX phases, a large number of 2D MXenes with unprecedented properties are expected to become available. Therefore, an important question to be answered at this moment is which of the MAX phases are promising candidates for a successful

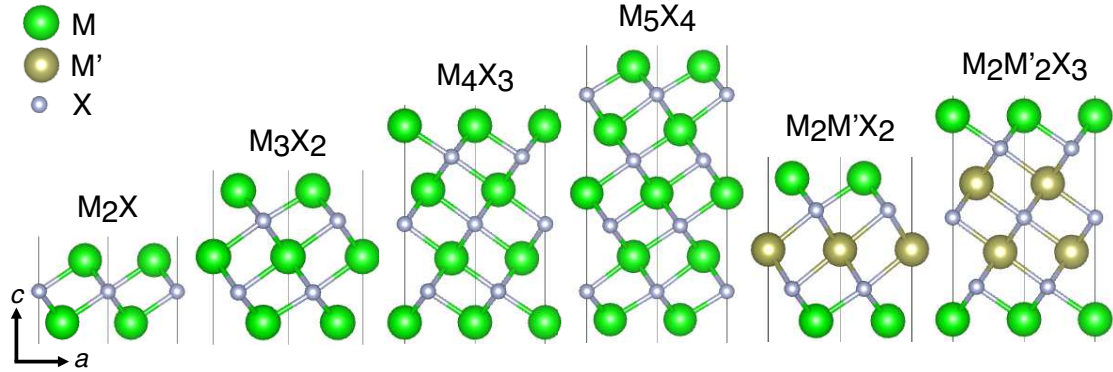


FIG. 2: Atomic structures of six different 2D MXenes. The a and c axes are common to all structures.

exfoliation into 2D materials. Theoretically, based on the analysis of tensile and shear stresses, the mechanical exfoliation of various M_2AlC ($M = Ti, Zr, Hf, V, Nb, Ta, Cr, Mo, and W$) MAX phases into 2D M_2C MXenes have been investigated.[68] There, it was found that by applying a large tensile strain, all the interlayer M-Al bonds can be broken, leading to the separation between M_2C and Al layers.[68] However, the chemical exfoliation process is a very complicated dynamical process, which is very difficult to model and simulate with all the details. Nevertheless, we can still gain great insights through studying the bond strength and the exfoliation energy because it is expected that MAX phases with weaker M-A bonds are promising for the successful exfoliation process. In this paper, by using a set of first-principles calculations based on density functional theory (DFT), we study the electronic structures, static exfoliation energies, force constants, and bond strengths of the 82 crystalline MAX phases. We show that the force constant is clearly correlated with the bond strength. We find that except for the MAX phases with the A elements of S or P, many of the MAX phases with other types of A elements have higher possibility for exfoliation into 2D MXenes. Moreover, we examine the effect of charge injection on the bond strength of the MAX phases. For negatively charged MAX phases, the M-A bonds become elongated and weaker upon receiving electrons, thus facilitating the exfoliation process. However, the exfoliation becomes harder for positively charged MAX phases.

II. METHODS OF CALCULATIONS

Among different methods, first-principles calculations based on density functional theory (DFT) have proven to be reliable to predict various physical and chemical phenomena on the atomic scale. Hence, we employ DFT calculations to optimize the atomic structures and investigate the electronic structures of the MAX phases. All calculations are performed using the Vienna ab initio simulation package (VASP) code.[69] The generalized gradient approximation (GGA) using the Perdew-

Burke-Ernzerhof (PBE) functional is used to compute the exchange-correlation energy.[70] The projected augmented wave approach with a plane wave cutoff energy of 520 eV is used to construct the wave functions. The atomic positions and lattice constants are fully optimized using the conjugate gradient method without imposing any symmetry. After structural optimization of atomic structures, the maximum residual force on each atom is less than 0.0001 eV/Å. In the electronic self-consistency procedure, the total energies are converged to within 10^{-8} eV/cell. For the optimization of $M_{n+1}AX_n$ ($M_2M'_nAX_{n+1}$), the Brillouin zone is sampled by taking $18 \times 18 \times 9$, $18 \times 18 \times 6$, $18 \times 18 \times 3$, and $18 \times 18 \times 1$ ($18 \times 18 \times 6$ and $18 \times 18 \times 3$) Monkhorst-Pack \mathbf{k} points [71] for $n = 1, 2, 3$, and 4 (for $n = 1$ and 2), respectively. To calculate the projected density of states (PDOS), we use a larger number of \mathbf{k} points, *i.e.*, $24 \times 24 \times 12$, $24 \times 24 \times 9$, $24 \times 24 \times 6$, and $24 \times 24 \times 3$ Monkhorst-Pack \mathbf{k} points for $n = 1, 2, 3$, and 4, respectively. Spin-polarized calculations are employed to optimize the atomic structures of neutral and charged MAX phases. We find that most of the MAX phases are nonmagnetic, except for a few Cr-based MAX phases that exhibit weak magnetism. The total energies of all optimized MXenes are evaluated using spin-polarized calculations.

The phonon calculations are carried out for nonmagnetic structures using the PHONOPY package [72] along with the VASP.[69] The force constant is the second derivative of the total energy with respect to finite displacements of atoms i and j along the x , y , and z directions, and is a 3×3 matrix, given as one of the output results of the phonon calculations. Since the trace of the force constant matrix is independent of the coordinate system, *i.e.*, invariant under a coordinate rotation,[73, 74] following ref.[74] we consider the trace of the force constant matrix and refer to this scalar quantity as the force constant F_{ij} between atoms i and j in the main text.

Crystal orbital Hamilton population (COHP) analysis is a technique for partitioning the band-structure energy into bonding, nonbonding, and antibonding contributions of the localized atomic basis sets.[75] Alternatively, the COHP may be described as a hopping-

weighted density-of-states between a pair of adjacent atoms defined as

$$\text{COHP}_{\mu\vec{T},\nu\vec{T}'}(E) = H_{\mu\vec{T},\nu\vec{T}'} \sum_{j,\vec{k}} f_j(\vec{k}) C_{\mu\vec{T},j}^*(\vec{k}) C_{\nu\vec{T}',j}(\vec{k}) \delta(\epsilon_j(\vec{k}) - E), \quad (1)$$

where $H_{\mu\vec{T},\nu\vec{T}'}$ is the matrix element of the Hamiltonian matrix H and $C_{\mu\vec{T},j}(\vec{k})$ represents the eigenvector coefficient of an atomic orbital μ . $\epsilon_j(\vec{k})$ is the j th band energy at momentum \vec{k} , \vec{T} is the translational lattice vector, and $f_j(\vec{k})$ is the occupation number of that state. Similar to the density of states (DOS) where the energy integration up to the Fermi energy gives the number of electrons, the energy integration of the COHP up to a particular band energy for a pair of atoms indicates their bond strength in terms of their contribution to this band structure energy. Upon integrating *all* COHPs including the on-site elements that correspond to a self-interaction of an atom, up to the Fermi energy, one is left with the integral of the density-of-energy (DOE) function, another partitioning of the band-structure energy.[76] All the COHP calculations are done using the Local Orbital Basis Suite Towards Electronic-Structure Reconstruction (LOBSTER) code [77–79] with the pbeVaspFit2015 basis set.[79]

The bond order (N) is calculated based on the Pauling classical descriptor $D_N = D_1 - \gamma \text{Å} \times \log_{10} N$, where D_1 and D_N are the length of a single bond and the measured bond length, respectively.[80, 81] D_1 for a X–Y bond is given as $D_1 = R_X + R_Y$, where R_X and R_Y are the single-bond radii of elements X and Y. In this formula, the coefficient γ can vary in the range between 0.6 and 0.7.[81] In our calculations, we set that $\gamma = 0.6$ in consistency with the previous studies in the literature.[82, 83] The lengths of single-bond radii of pure metals have already been tabulated for most elements.[80, 81, 84]

The elastic constant C_{33} is obtained by parabolically fitting the total energy of the strained crystal along the c direction with respect to small distortions ($\Delta c/c = \pm 0.02, \pm 0.015, \pm 0.01$, and ± 0.005).[85] The static exfoliation energy $E_{\text{Exfoliation}}$ of a bulk MAX phase into 2D MXenes is calculated through $E_{\text{Exfoliation}} = -[E_{\text{tot}}(\text{MAX phase}) - 2 E_{\text{tot}}(\text{MXene}) - 2 E_{\text{tot}}(\text{A})]/(4S)$, where $E_{\text{tot}}(\text{MAX phase})$, $E_{\text{tot}}(\text{MXene})$ and $E_{\text{tot}}(\text{A})$ stand for the total energies of bulk MAX phase, 2D MXene, and A element, respectively.[14]. Here, $S = \sqrt{3}a^2/2$ is the surface area and a is the lattice parameter of the MAX phase. Exfoliating a MAX phase, each unit cell of the MAX phase generates two MXene layers with totally 4 surfaces. Hence, the exfoliation energy is divided by 4 in the above formula. The total energy of A element, $E_{\text{tot}}(\text{A})$, is estimated from its most stable bulk structure.

III. RESULTS AND DISCUSSION

In experiments, the exfoliation process occurs dynamically and there are many parameters to control the process, such as the acidic solution type, the concentration

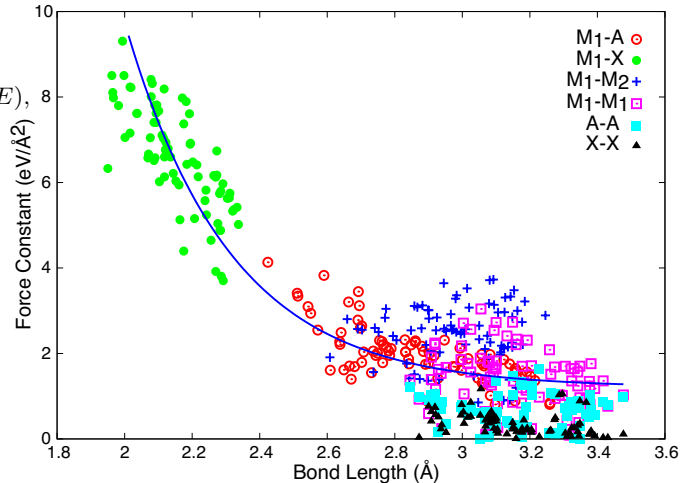


FIG. 3: Calculated force constants of different bonds versus the corresponding bond lengths for the 82 experimentally synthesized MAX phases. The line is a guide to the eye.

of the acid, and the temperature. However, it is very difficult, if not impossible, to theoretically consider all these details of the process using the currently available computational resources, although there have been several attempts to look into such a complicated process in the literature.[86, 87] Therefore, currently, the static calculations are considered as the only straightforward way to provide useful information on the exfoliation possibility. In this regard, force constants, integrated crystal orbital Hamilton population (ICOHP), bond orders, and exfoliation energies are important quantities that can provide quantitative measures of the bond strength and the ease of exfoliation. This simulation-based approach is highly valuable since the bond strength is not an experimentally measurable quantity (except for diatomic molecules) but nonetheless it is chemically meaningful.

A. Force constant analysis

The force constant is the second derivative of the total energy with respect to the displacement of an atom, which is also equivalent to the first derivative of the force. It represents the force required to displace an atom by an infinitesimal amount while all other atoms are held fixed in their equilibrium positions. Because of this, the force constant has been used as a bond strength descriptor in the literature.[88–90] Historically, the force constant has been used to describe the strength of a bond in terms of dissociation, particularly applied to investigate the dissociation energy of atomic dimers.[91] While the binding energy is the energy required to dissociate a bond from its equilibrium position, the force constant is the curvature of the energy vs. bond length curve at the equilibrium position. Although in general the binding energy and the force constant are not mathematically

TABLE I: List of MAX phases exfoliated experimentally into MXenes and the calculated exfoliation energy $E_{\text{Exfoliation}}$ (eV/Å²) and total force constant FC_i (eV/Å²) for an i (= M, A, or X) atom counting all contributions from the neighboring atoms.

MAX Phase	FC_M	FC_A	FC_X	$E_{\text{Exfoliation}}$
Ti ₂ AlC[29]	46.742	15.078	51.518	0.164
Ti ₂ AlN[30]	45.139	18.813	50.626	0.190
V ₂ AlC[31]	51.943	21.855	59.168	0.205
Nb ₂ AlC[31]	51.706	18.205	49.187	0.185
Ti ₃ AlC ₂ [28]	49.175	14.708	49.514	0.158
Zr ₃ AlC ₂ [33]	46.019	11.886	40.511	0.131
Ti ₄ AlN ₃ [36]	48.502	19.080	51.258	0.193
Nb ₄ AlC ₃ [34]	53.323	16.680	48.319	0.175
Ta ₄ AlC ₃ [29]	53.959	18.618	55.066	0.197
Mo ₂ ScAlC ₂ [7]	45.170	20.251	44.822	0.201
Mo ₂ TiAlC ₂ [37]	49.797	20.086	52.324	0.196
Cr ₂ TiAlC ₂ [37]	44.253	20.124	53.691	0.184
Mo ₂ Ti ₂ AlC ₃ [37]	51.522	20.094	52.379	0.199

related directly, it is easy to conceive that when the binding is weak, the curvature of the energy vs. bond length curve is small, and vice versa, namely, when the curvature is large, the binding is strong. A very simple justification for this relation between the binding energy and the force constant can be found when the energy scale of the interatomic interaction potential has a Morse [92] or Lennard-Jones potential form.[93] While both quantities can easily be calculated for molecules, in the case of solids, it is impossible to consider the energy change when only one bond is stretched, but we rather consider the cohesive energy where *all* bonds are stretched. Therefore, it is preferable to discuss the bond strength based on the force constant, which one can calculate theoretically even for solids. Moreover, in recent years, the concept of a force constant descriptor has been developed to investigate the strength of interactions in solids [74, 94] and interfaces.[95, 96] For the case of Sb₂Se₃, for example, it was found that there is a clear correlation between the stiffness of a particular bond (expressed by the force constant) and the covalency (expressed by COHP analysis).[82] This motivates us to investigate the bond strength in the MAX phases from the view point of the force constant.

In order to evaluate the force constants of the bonds in MAX phases, we perform a set of phonon calculations on the 82 experimentally crystalline MAX phases, listed in Table 1S. As expected and consistent with the experimental results, no negative phonon frequencies are found in the phonon spectra of these MAX phases. This indicates that these MAX phases are dynamically stable. The phonon spectra calculated here are given in the supporting information file. Table 1S includes the results of the force constants for M₁–M₁, M₁–M₂, M₁–X, M₁–A, A–A, and X–X bonds. Here, M₁ and M₂ represent tran-

TABLE II: List of MAX phases sorted with FC_A (≤ 21.855 eV/Å²) in ascending order (from top left to bottom right). The calculated FC_A (eV/Å²) is shown in each parenthesis. The results for all studied MAX phases are provided in the supporting information file.

Sc ₂ GaC (5.590)	Sc ₂ AlC (6.412)	Sc ₂ InC (8.771)
Sc ₂ TiC (9.628)	Ti ₂ CdC (11.683)	Zr ₂ AlC (11.852)
Zr ₃ AlC ₂ (11.886)	Ti ₃ AuC ₂ (12.108)	Ti ₅ AlC ₄ (12.395)
Zr ₂ InC (13.475)	Zr ₂ TiC (13.693)	Hf ₂ AlC (13.999)
Ti ₂ GaC (14.594)	Ti ₄ GaC ₃ (14.668)	Ti ₃ AlC ₂ (14.708)
Zr ₂ AlN (15.047)	Ti ₂ AlC (15.077)	Hf ₂ InC (15.64)
Nb ₅ AlC ₄ (15.724)	Hf ₂ TiC (16.117)	Zr ₂ InN (16.327)
Zr ₂ TiN (16.380)	Zr ₂ PbC (16.658)	Nb ₄ AlC ₃ (16.680)
Ti ₂ InC (17.174)	Hf ₂ AlN (17.288)	Ti ₂ TiC (17.438)
Nb ₂ GaC (17.520)	Zr ₂ SnC (17.769)	Ti ₂ GaN (17.942)
Nb ₂ AlC (18.205)	Zr ₂ BiC (18.344)	Ta ₅ AlC ₄ (18.364)
Hf ₂ PbC (18.518)	Ta ₄ AlC ₃ (18.618)	Ti ₃ SiC ₂ (18.786)
Ti ₄ SiC ₃ (18.801)	Ti ₂ AlN (18.813)	Ti ₃ GeC ₂ (18.867)
Nb ₂ InC (18.884)	Ti ₂ GeC (19.016)	Ti ₄ AlN ₃ (19.08)
Ti ₄ GeC ₃ (19.118)	Hf ₂ SnC (19.217)	Mo ₂ GaC (19.247)
Ti ₂ SiC (19.366)	Ta ₂ GaC (19.464)	Cr ₂ GaN (19.492)
Ti ₃ IrC ₂ (19.702)	V ₂ GaC (19.803)	Ti ₂ InN (19.971)
Mo ₂ TiAlC ₂ (20.086)	Mo ₂ Ti ₂ AlC ₃ (20.094)	V ₂ GaN (20.107)
Cr ₂ TiAlC ₂ (20.124)	Mo ₂ ScAlC ₂ (20.251)	Ta ₂ AlC ₂ (20.536)
Ti ₂ PbC (20.543)	Ta ₂ AlC (20.596)	Cr ₂ GaC (20.775)
V ₄ AlC ₃ (20.866)	V ₃ AlC ₂ (20.894)	Hf ₂ SnN (21.213)
Ti ₂ SnC (21.586)	V ₂ AlC (21.855)	

sition metals belonging to the first and second layers of transition metals close to the A element, and the X layer is sandwiched between M₁ and M₂ layers (see Fig. 1). In M₂AX, M₃AX₂, M₄AX₃, and M₅AX₄ MAX phases, the transition metals of M₁ and M₂ are of the same type, while in M₂M'AX₂ and M₂M'₂AX₃ MAX phases, M₁ and M₂ are of different types. The results of the force constants for these bonds are summarized in Fig. 3. A general trend can be revealed that shorter bonds are stiffer. It is also observed that the force constants of the M₁–X bonds are significantly larger than those of other bonds. This indicates that the M₁–X bonds are the strongest in the MAX phases, which is the main reason for the stability of these MAX phases and the resulting MXenes. Since the force constants of the M₁–A bonds are smaller than those of the M₁–X bonds, implying that the M₁–A bonds are weaker than the M₁–X bonds, it is expected that the bulk modulus of MAX phases is not larger than that of their corresponding binary MX compounds. This is consistent with previous studies where the bulk modulus of M₂AX MAX phases was classified into two groups, a group with a similar bulk modulus and a group with a smaller bulk modulus as compared to that of the binary MX compounds.[97, 98]

As shown in Fig. 3, the force constants of the M₁–M₂ bonds are as large as those of the M₁–A bonds but

TABLE III: List of MAX phases sorted by FC_X (≥ 40.511 eV/Å 2) in descending order (from top left to bottom right). The calculated FC_X (eV/Å 2) is shown in each parenthesis. The results for all studied MAX phases are provided in the supporting information file.

V_2AlC (59.168)	V_2GaC (58.198)	V_4AlC_3 (58.123)
Cr_2AlC (57.783)	Ta_2AlC (57.183)	Ta_3AlC_2 (55.922)
V_3AlC_2 (55.760)	Ta_2GaC (55.684)	Ta_4AlC_3 (55.066)
V_2SiC (54.431)	Cr_2GaC (53.940)	Cr_2TiAlC_2 (53.691)
Cr_2GeC (53.649)	$Mo_2Ti_2AlC_3$ (52.379)	Mo_2TiAlC_2 (52.324)
Ta_5AlC_4 (53.042)	V_2GeC (52.022)	Ti_2AlC (51.518)
Ti_2SiC (51.315)	V_3SiC_2 (51.296)	Ti_4AlN_3 (51.258)
Ti_2GaC (50.935)	Ti_3IrC_2 (50.703)	Ti_2AlN (50.626)
Ti_2GaN (50.307)	V_2PC (49.711)	Ti_3SiC_2 (49.697)
Ti_3AlC_2 (49.514)	Ti_2GeC (49.400)	Nb_2AlC (49.187)
Ti_2GeC_2 (48.641)	Nb_2GaC (48.560)	Nb_4AlC_3 (48.319)
V_2GaN (48.010)	Ti_4SiC_3 (47.710)	Ti_3AuC_2 (47.647)
Ti_2CdC (47.573)	Ti_4GaC_3 (47.563)	Ti_2InC (47.441)
V_2AsC (47.374)	Cr_2GaN (47.339)	Hf_2AlC (47.038)
Ti_4GeC_3 (46.894)	Mo_2GaC (46.103)	Ti_2TiC (45.923)
Ti_5AlC_4 (45.731)	Ti_3SnC_2 (45.549)	Hf_2InC (45.447)
Nb_5AlC_4 (45.336)	Nb_2InC (45.318)	Ti_2SC (45.014)
Mo_2ScAlC_2 (44.822)	Hf_2TiC (44.767)	Ti_2SnC (44.679)
Ti_2InN (44.642)	Hf_2SC (44.560)	Hf_2SnC (43.319)
Nb_2SC (42.841)	Hf_2AlN (42.212)	Hf_2PbC (41.947)
Ti_2PbC (41.906)	Nb_2PC (41.902)	Nb_2SnC (41.843)
Zr_2AlC (41.725)	Nb_3SiC_2 (41.391)	Ti_2AsC (41.355)
Nb_2AsC (40.670)	Zr_2InC (40.623)	Zr_3AlC_2 (40.511)

smaller than those for the M_1-X bonds. This suggests that the M_1-M_2 bonds are also weaker or softer than the M_1-X bonds, which is in agreement with chemical intuition. However, the M_1-A and M_1-M_2 bonds are still strong enough to contribute to the stability of MAX phases. Because of the periodicity of the structure, the lengths of the M_1-M_1 , $A-A$, and $X-X$ bonds are equal to the lattice constant a , which is larger than the lengths of the M_1-X , M_1-A , or M_1-M_2 bonds. Since the $X-X$ interatomic distances are more than two times larger than the atomic radii of X elements, the orbital overlap between the X atoms in the $X-X$ bonds should be weak. On the other hand, twice the atomic radii of A or M atoms are comparable with the $A-A$ or M_1-M_1 bond lengths, suggesting that the A or M atoms in the $A-A$ or M_1-M_1 bonds exhibit strong orbital overlap. Therefore, we expect the $X-X$ bonds to be the weakest among all the bonds, as observed in Fig. 3 and Table 1S.

In order to exfoliate MAX phases into 2D MXenes, the bonds between an A atom and its neighboring A or M atoms have to be broken. In other words, to detach an A atom from the bulk MAX phase, at least six $A-A$ bonds and six M_1-A bonds must be broken. Hence, to propose which of the MAX phases can be exfoliated to MXenes, here we calculate the total force constants for an i (=

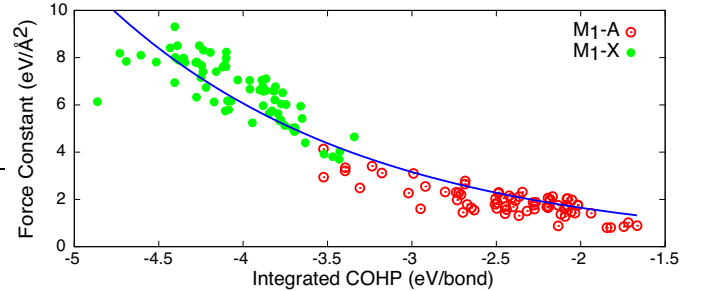


FIG. 4: Bond strength versus force constant for the M_1-A and M_1-X bonds for various experimentally synthesized MAX phases. Here the bond strength is quantified by the integrated crystal orbital Hamilton population (COHP) up to the Fermi energy over all the atomic orbital interactions between the atoms forming the bonds. The line is a guide to the eye.

M , A , or X) atom counting all contributions from other atoms, *i.e.*, $FC_i = \sum_j FC_{ij}$, where FC_{ij} is the force constant between atoms i and j , and j enumerates all atoms in the supercell of the phonon calculation except atom i . Generally, the force constant is a 3×3 second-order tensor and here we consider the trace of this tensor as FC_{ij} . Therefore, FC_i is related to the second derivative of the total energy E with respect to displacement $r_i^{(\alpha)}$ (where $\alpha = x, y, z$) of atom i in the α direction, *i.e.*, $FC_i = \sum_\alpha \partial^2 E / \partial^2 r_i^{(\alpha)}$. After the systematic calculation (see the results in Table 1S), we find that in most of the MAX phases the force constants between an A atom and the surrounding atoms located further than the first shell of neighbors are weak. Therefore, an A atom mainly interacts with the neighboring atoms in its first shell of neighbors, which are of the M or A atoms. We also find that the total force constants of an X or M atom are significantly larger than those of an A atom (see Table I and Table 1S). This explains why in the exfoliation process the bonds formed by M and A atoms are typically broken rather than those formed by M and X atoms.

In order to examine which of the MAX phases are well-suited for the successful exfoliation into 2D MXenes, the total force constant FC_A for the A elements is a very useful quantity. As a simple criterion, we can expect that MAX phases with smaller FC_A can be considered as promising candidates for the exfoliation process. In this respect, Ti_2AlC , V_2AlC , Ti_3AlC_2 , Zr_3AlC_2 , Ti_4AlN_3 , Nb_4AlC_3 , Mo_2TiAlC_2 , Cr_2TiAlC_2 , Mo_2ScAlC_2 , and $Mo_2Ti_2AlC_3$ are the list of MAX phases that have already been exfoliated to Ti_2C , V_2C , Ti_3C_2 , Zr_3C_2 , Ti_4N_3 , Nb_4C_3 , Mo_2TiC_2 , Cr_2TiC_2 , Mo_2ScC_2 , and $Mo_2Ti_2C_3$, respectively. All these compounds contain Al in the MAX phases. The calculated FC_A values in these compounds are summarized in Table I. As shown in Table I, the minimum (maximum) FC_A is for Zr_3AlC_2 (V_2AlC). Therefore, we expect that by using appropriate acids in the experiments it might be possible to break the bonds as strong as the $V-Al$ bond. Based on this crite-

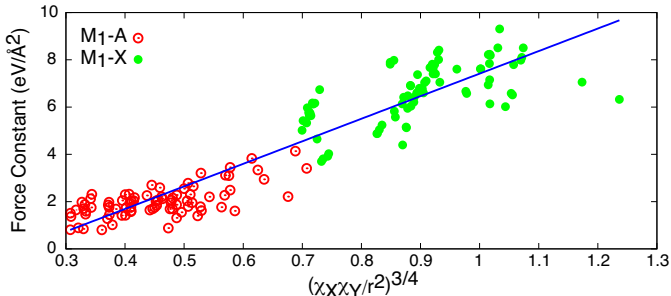


FIG. 5: Force constant of the M_1-A and M_1-X bonds as a function of electronegativities for various experimentally synthesized MAX phases. χ_X and χ_Y , and r are the electronegativities of X and Y atoms, and the length of the $X-Y$ bond. The straight line is a guide to the eye.

tion, we screen our data in Table 1S for compounds with FC_A less than $21.855 \text{ eV}/\text{\AA}^2$ and the results are summarized in Table II. The compounds listed in Table II are sorted based on their FC_A values in ascending order: the smaller FC_A is, the higher the chance for successful exfoliation becomes. Therefore, the table lists the compounds from the most promising candidate to the least promising one for successful exfoliation. However, it is noted that all compounds listed in Table II have better potential to be exfoliated into MXenes because their respective FC_A is below the upper limit of $21.855 \text{ eV}/\text{\AA}^2$.

The exfoliation process would be successful experimentally only if the obtained 2D MXenes are structurally perfect. This requires that the M_1-M_1 , M_1-M_2 , and M_1-X bonds should be stronger than the M_1-A and $A-A$ bonds. Otherwise, during the exfoliation process, other bonds may also be broken besides the M_1-A bonds. In such a case, either the MXenes would not be formed at all or they would be formed with many M and X defects. Since the M_1-X bonds are the strongest in MAX phases, we calculate the total force constant FC_X for the X elements in Table I for the MAX phases experimentally exfoliated into MXenes. We find that the maximum (minimum) of FC_X is for V_2AlC (Zr_3AlC_2). Therefore, in order to successfully synthesize MXenes, FC_X should at least be as large as that for Zr_3AlC_2 (40.511 eV/Å²). Based on this criterion, we re-screen the results of FC_X in all MAX phases listed in Table 2S and the results are summarized in Table III. The compounds listed in Table III are sorted based on their FC_X values in descending order: the larger FC_X is, the higher the quality of the obtained MXene is expected once it is successfully exfoliated.

The results shown in Table 1S are also helpful to predict which of the MAX phases have the least chance for successful exfoliation into 2D MXenes. It is found in Table 1S that in MAX phases with the A elements being P or S, the M_1-P or M_1-S bonds are as strong as the M_1-X bonds. This suggests that charge neutral MAX phases with A = S or P are typically less promising com-

pounds for the exfoliation process. Another important implication of the results shown in Table II is a possibility of MAX phases for ion intercalation and their use for applications such as Li ion batteries.[99, 100] Because of the weaker bond strength of the M_1 –A bonds as compared with the M_1 –X bonds, and the greater interatomic distances, MAX phases possess large free space near A atoms. It can be inferred that the guest ions should be intercalated near the A atoms. Therefore, MAX phases with weaker strength of the M_1 –A bonds might find better applications in Li ion batteries.

B. Bond strength analysis

From a chemical point of view, the bond strength of a covalent interaction depends on the overlap between the atomic orbitals of the two atoms that form a bond. Somewhat simplified, the polarity of the bond results from the electronegativity difference between the two atoms connected by the bond [101]. Typically, the overlap decreases exponentially with the bond length.[101] The electronegativity difference of the two atoms forming the bond also determines the effective charges on the atoms in the $\frac{1}{r}$ potential.[101] As explained in the section of methods of calculations, the integrated crystal orbital Hamilton population (COHP) up to the Fermi energy measures the mixing (*i.e.*, the amount of interactions) of atomic orbitals, eventually determining the bond strength, and the COHP method has been widely applied to a plethora of materials,[102] including MAX phases.[103]

Here, we calculate the integrated COHP (ICOHP) up to the Fermi energy over all the atomic orbital interactions between the atoms forming the bonds. Figure 4 shows the force constant versus the bond strength quantified by the ICOHP for the M_1-X and M_1-A bonds. Note that the more negative (*i.e.*, the more energy-lowering) the ICOHP is, the stronger the bond is. It is clearly observed in Fig. 4 that the force constant intimately correlates with the strength of bonds: the force constant increases with increasing the bond strength. It is also found that the mixing of orbitals in the M_1-X bonds is larger than that in the M_1-A bonds. Both M_1-X and M_1-A bonds are polar because the electronegativities χ_{M_1} , χ_A , and χ_X of the M_1 , A, and X elements are different. Generally, the polarity of the M_1-X bonds (*i.e.*, $\chi_{M_1} - \chi_X$) is larger than that of the M_1-A bonds (*i.e.*, $\chi_{M_1} - \chi_A$). Therefore, in addition to the orbital interaction, the ionic effect may also play a role in determining the difference of the stiffness between the M_1-X and M_1-A bonds.

There is no well-developed formalism to isolate the contribution of polarity of the bond to the force constant, except for extracting the ionicity (as well as the orbital mixing) from modern DFT-type PAW wave functions, *e.g.*, in the search for advanced materials via materials mapping.[104] Here, we rely on an empirical model pro-

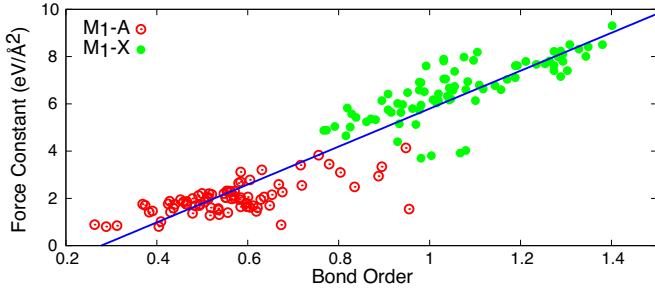


FIG. 6: Force constant of the M_1 –A and M_1 –X bonds as a function of the corresponding Pauling bond order, calculated for various experimentally synthesized MAX phases. The straight line is a guide to the eye.

posed for molecules,[105–107] *i.e.*, the force constant (k) of diatomic molecules, $k = aN(\chi_X\chi_Y/r^2)^{3/4} + b$, where a and b are constants, χ_X and χ_Y stand for the electronegativities of X and Y atoms, respectively, r is the X–Y bond length, and N is the number of bonds (bond order, $N = 1, 2$, and 3) between X and Y atoms.[105, 106] The physics behind the empirical model can be easily understood because the amount of charge on the nuclei is related to the electronegativities of the the bonded atoms, and the force F between a nucleus and an electron in the bonded atoms can be estimated from the simple rule of electrostatic point charge.[108] From Hooke’s law $F = -k\Delta r$, the attractive force between the two bonded atoms is related to the force constant k , where Δr is the change in the bond length. Hence, the overall dependence of the force constant on the electronegativities and the bond distance can be justified. In this empirical model, the parameters a , N , and b are found through a fitting process. Figure 5 shows the force constant, calculated in Fig. 3, as a function of $(\chi_X\chi_Y/r^2)^{3/4}$. Although the empirical model is a very rough approximation, it can still capture the physics of the polar bond in MAX phases. We find that $(\chi_X\chi_Y/r^2)^{3/4}$ varies almost linearly with the force constant and it is larger for the M_1 –X bonds than the M_1 –A bonds. The latter indicates that in addition to the orbital interaction, the polarity plays an important role in the stiffness of the M_1 –X bonds.

C. Bond order analysis

In chemistry, the total number of bonds ($N = 1, 2$, and 3) between bonded atoms, the so-called bond order, is usually assigned to represent the strength of a bond. It is considered that the bond becomes stronger with increasing bond order. For instance, in the literature, the carbon–carbon bonds are categorized as single, double, or triple-bonds in various compounds when the carbon–carbon bond distances are around 1.542, 1.339, and 1.204 Å, respectively. As described in the methodology section, Pauling has proposed an empirical logarithmic model to describe the bond order.[80, 81] Based on the Pauling for-

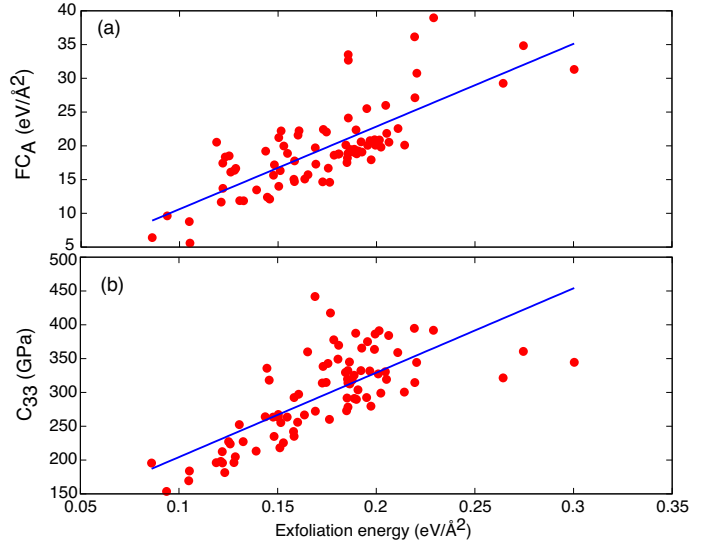


FIG. 7: (a) Force constant FC_A for the A atoms and (b) elastic constant C_{33} along the c direction versus exfoliation energy $E_{\text{Exfoliation}}$ ($\text{eV}/\text{\AA}^2$), calculated for various experimentally synthesized MAX phases. The straight lines in (a) and (b) are guides to the eye.

mula along with the metallic radii of elements provided in Ref. [81], we calculate in Fig. 6 the force constants of the M_1 –A and M_1 –X bonds with respect to their corresponding bond orders in various MAX phases. It is clearly found that as the bond order increases, the force constant also increases. The bond orders for the M_1 –X bonds are larger than that for the M_1 –A bonds, thus indicating that the M_1 –X bonds are stronger than the M_1 –A bonds, which is consistent with the COHP analysis given above. Moreover, it is observed in Fig. 6 that the bond orders for the M_1 –A bonds are less than 1. This suggests that the bond strength of the M_1 –A bonds is weaker than the single bonds in pure metals of A and M. We have repeated the same analysis using the single bond radii given in Ref. [84] and obtained the same conclusion (see supplementary data).

D. Exfoliation energy analysis

As we described above, the chemical exfoliation is a complicated dynamical process with subtle details. Hence, it is extremely difficult to simulate such processes computationally. However, the calculation of the static exfoliation energy would help us to screen MAX phases for the successful exfoliation process into 2D MXenes. Here, we evaluate the exfoliation energy $E_{\text{Exfoliation}}$ for the 82 different MAX phases summarized in Table 2S. The definition of $E_{\text{Exfoliation}}$ is given in the section of methods of calculations. As shown in Table I, among the MAX phases experimentally exfoliated into MXenes, Zr_3AlC_2 (V_2AlC_2) shows the lowest (largest) $E_{\text{Exfoliation}}$ (eV/area), 0.131 (0.205) $\text{eV}/\text{\AA}^2$. Therefore, we expect

TABLE IV: List of MAX phases sorted by the exfoliation energy $E_{\text{Exfoliation}}$ (eV/Å²) (≤ 0.205 eV/Å²) in ascending order (from top left to bottom right). The results for all studied MAX phases are provided in the supporting information file.

Sc ₂ AlC (0.086)	Sc ₂ TiC (0.094)	Sc ₂ InC (0.105)
Sc ₂ GaC (0.105)	Ti ₂ PbC (0.119)	Ti ₂ CdC (0.121)
Ti ₂ TiC (0.122)	Zr ₂ TiC (0.122)	Zr ₂ BiC (0.123)
Hf ₂ PbC (0.125)	Hf ₂ TiC (0.126)	Zr ₂ TiN (0.128)
Zr ₂ PbC (0.129)	Zr ₃ AlC ₂ (0.131)	Zr ₂ AlC (0.133)
Zr ₂ InC (0.139)	Hf ₂ SnC (0.144)	Ti ₅ AlC ₄ (0.145)
Ti ₃ AuC ₂ (0.146)	Hf ₂ InC (0.148)	Ti ₂ InC (0.148)
Hf ₂ AlC (0.150)	Hf ₂ SnN (0.150)	Zr ₂ InN (0.151)
Nb ₂ SnC (0.152)	Ti ₂ InN (0.153)	Nb ₂ InC (0.155)
Zr ₂ AlN (0.158)	Ti ₃ AlC ₂ (0.158)	Zr ₂ SnC (0.158)
Ti ₂ SnC (0.160)	Ti ₃ SnC ₂ (0.161)	Ti ₂ AlC (0.164)
Nb ₅ AlC ₄ (0.165)	Ti ₃ IrC ₂ (0.169)	Hf ₂ AlN (0.169)
Ti ₄ GaC ₃ (0.173)	Cr ₂ GeC (0.173)	Nb ₃ SiC ₂ (0.175)
Nb ₄ AlC ₃ (0.175)	Ti ₂ GaC (0.176)	Ta ₅ AlC ₄ (0.177)
Ti ₃ SiC ₂ (0.181)	Ti ₄ SiC ₃ (0.181)	Cr ₂ TiAlC ₂ (0.184)
Nb ₂ GaC (0.185)	Nb ₂ AlC (0.185)	Ti ₃ GeC ₂ (0.186)
Nb ₂ AsC (0.186)	V ₂ GeC (0.186)	V ₂ AsC (0.186)
Ti ₄ GeC ₃ (0.186)	Ta ₂ GaC (0.187)	Ti ₂ SiC (0.188)
Cr ₂ GaN (0.189)	Ti ₂ GeC (0.189)	V ₃ SiC ₂ (0.190)
Ti ₂ AlN (0.190)	Mo ₂ GaC (0.191)	Ta ₂ AlC (0.192)
Ti ₄ AlN ₃ (0.193)	Ti ₂ AsC (0.195)	Mo ₂ TiAlC ₂ (0.196)
Cr ₂ GaC (0.197)	Ti ₂ GaN (0.197)	V ₃ AlC ₂ (0.199)
Mo ₂ Ti ₂ AlC ₃ (0.199)	Mo ₂ ScAlC ₂ (0.200)	V ₄ AlC ₃ (0.201)
V ₂ GaC (0.202)	V ₂ SiC (0.205)	V ₂ AlC (0.205)

that the MAX phases with an exfoliation energy lower than 0.205 eV/Å² have a better chance to be exfoliated into MXenes. These MAX phases are listed in Table IV. The compounds listed in Table IV are sorted based on their exfoliation energies in ascending order: the smaller the exfoliation energy is, the better the chance for successful exfoliation becomes. Therefore, the table lists the compounds from the most promising candidate to the least promising one for successful exfoliation. Figure 7(a) shows the total force constant FC_A for the A atoms versus the exfoliation energy. It is clearly observed that the total force constant FC_A is strongly correlated with the exfoliation energy: the MAX phases with smaller FC_A have a lower exfoliation energy.

Because of the correlation between the force constant FC_A and the exfoliation energy, one would immediately expect a similar correlation with the elastic constant C_{33} along the c direction. This is simply because the M₁–A bonds are almost parallel to the c axis and thus C_{33} should be related to the force constant FC_A . Therefore, we calculate the elastic constants C_{33} for all MAX phases. As shown in Fig. 7(b), we indeed find that C_{33} is correlated with the exfoliation energies. This suggests that MAX phases with smaller (larger) C_{33} are easier (more difficult) to be exfoliated into 2D MXenes. How-

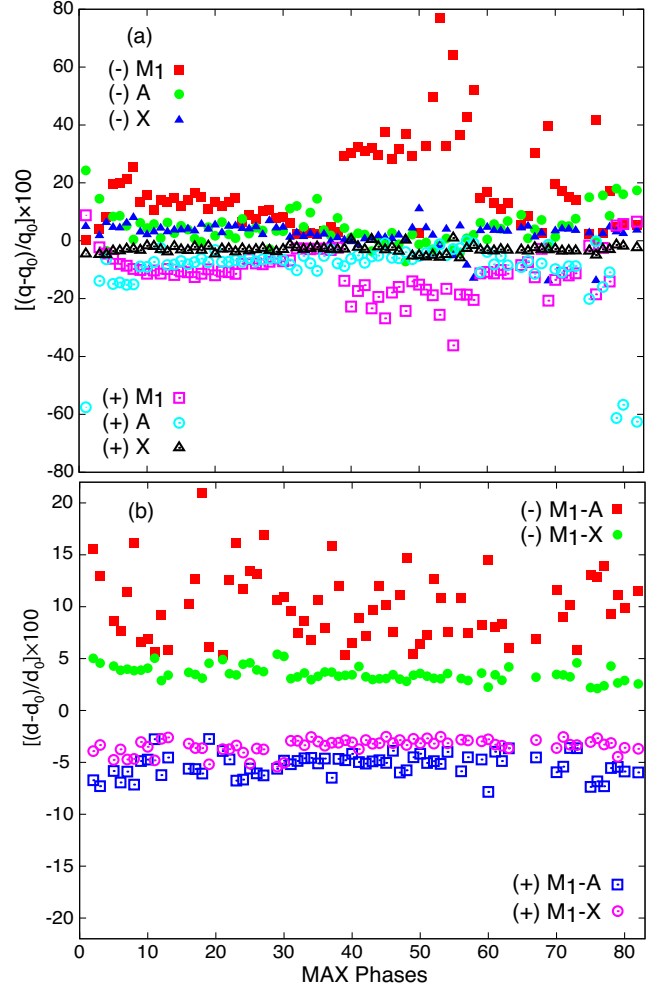


FIG. 8: (a) The relative amount of charge acquired by each element of the 82 experimentally synthesized MAX phases. q (q_0) represents the amount of charge on the M, A, and X atoms in the charged (neutral) MAX phases. (b) The relative change of length of the M₁–A and M₁–X bonds for the 82 experimentally synthesized MAX phases. d (d_0) denotes the bond distance in the charged (neutral) MAX phases. Plus (minus) sign in parenthesis indicates the positively (negatively) charged MAX phases. The numbers 1–82 in the horizontal axis represents the experimentally synthesized MAX phases, listed in Table 1S.

ever, we note that C_{33} should be used as a criterion for the exfoliation with care, because when the numbers of M and X layers are larger in the unit cell, as in $M_{n+1}AX_n$ ($n = 2 - 4$) MAX phases, the force constants for M and X atoms should also be relevant for C_{33} and thus the correlation between C_{33} and the exfoliation energy becomes weak. In any case, our finding here is important since C_{33} is an experimentally measurable quantity.

E. Best candidates

Combining all the analyses, we can finally conclude that the best candidates of MAX phases for the successful exfoliation into 2D MXenes are those MAX phases that are common in Tables II, III, and IV, *i.e.*, MAX phases with small total force constants of the A atoms, large total force constants of the M and X atoms, and low exfoliation energy. We predict that in addition to the 10 MAX phases that have already been exfoliated experimentally (listed in Table I), the following 37 MAX phases are promising candidates for the successful exfoliation. Since the exfoliation energy is more directly related to the chemical exfoliation process than the other two criteria, we prioritize this criterion to sort these 37 promising candidates from the smallest to the largest exfoliation energies. Therefore, in the following list, we predict that the first (last) MAX phase is the most (least) promising candidate for successful exfoliation: 1) Ti_2CdC , 2) Zr_2AlC , 3) Ti_3AuC_2 , 4) Ti_5AlC_4 , 5) Zr_2InC , 6) Hf_2AlC , 7) Ti_2GaC , 8) Ti_4GaC_3 , 9) Hf_2InC , 10) Nb_5AlC_4 , 11) Hf_2TlC , 12) Ti_2InC , 13) Ti_2TlC , 14) Nb_2GaC , 15) Hf_2PbC , 16) Ta_5AlC_4 , 17) Ti_3SiC_2 , 18) Ti_4SiC_3 , 19) Ti_3GeC_2 , 20) Nb_2InC , 21) Ti_2GeC , 22) Ti_4GeC_3 , 23) Hf_2SnC , 24) Mo_2GaC , 25) Ti_2SiC , 26) Ta_2GaC , 27) Cr_2GaN , 28) Ti_3IrC_2 , 29) V_2GaC , 30) Ti_2InN , 31) Ta_2AlC_2 , 32) Ti_2PbC , 33) Ta_2AlC , 34) Cr_2GaC , 35) V_4AlC_3 , 36) V_3AlC_2 , and 37) Ti_2SnC .

F. Effect of charging

In order to investigate the effects of electron (hole) injection to the MAX phases, here we add (remove) 2, 3, 4, and 5 electrons per unit cell to (from) M_2AX , M_3AX_2 , M_4AX_3 , and M_5AX_4 , respectively by changing the total number of valence electrons. The number of injected charges is chosen such that the number of injected charges per atom in all the studied MAX phases is the same. There are two options to analyze the charge distribution. One is the integration of PDOS up to the Fermi level, in which the eigenstates are projected onto atomic orbitals that are defined in the pseudopotentials and thus do not form a complete basis. Therefore, the charge conservation is violated in a sense that the number of electrons on the atoms is not found correctly. The second option, which satisfies the charge conservation, is the Bader charge analysis, based on a real-space grid.[109–111] We adopt the second option for our charge analysis.

Figure 8(a) shows the relative number of electrons or holes received by the M, A, and X atoms in the charged MAX phases with respect to the neutral ones. Interestingly, in both positively and negatively charged MAX phases, most of the charges are received by the transition metals. That suggests that the states close to the Fermi energy must be transition-metal-centered. In order to explore this observation, we calculate the electronic structure of the charged and neutral MAX phases. Typical re-

sults for the projected density of states for charged and neutral Zr_2TlC and Hf_2SC are shown in Fig. 9. More results are provided in the supporting information file for various MAX phases, including Zr_2TlN , Ti_3AuC_2 , Nb_4AlC_3 , Ti_5AlC_4 , Mo_2ScAlC_2 , and $Mo_2Ti_2AlC_3$. It is found that in all neutral MAX phases, the states near the Fermi energy are dominated by *d* orbitals of the transition metals, as anticipated already. Hence, the electrons or holes injected into the MAX phases are mainly received by the transition metals. Among Zr_2TlC and Hf_2SC , Hf atoms in Hf_2SC receive a larger number of electrons or holes as compared with Zr atoms in Zr_2TlC . This is simply because in Hf_2SC the states below and above the Fermi energy are almost purely contributed by the *d* orbitals of Hf, while in the case of Zr_2TlC , in addition to the *d* orbitals of Zr, there is a contribution from the *d* orbitals of Tl near the Fermi energy.

In order to investigate the effect of charge injection on the bonds, we calculate in Fig. 8(b) the relative change of the M_1 –A and M_1 –X bond lengths. It is found that in the positively (negatively) charged MAX phases, the bond lengths of both M_1 –A and M_1 –X bonds decrease (increase). By injecting electrons (holes), the number of electrons on the M, A, or X atoms increases (decreases), which results in a longer (shorter) bond length. Interestingly, the impact of the charge injection on the M_1 –A bonds is generally more significant than that on the M_1 –X bonds. The results for the M_1 –A bond elongation with the electron injection are summarized in Table V. When the transition metals receive a sufficient amount of electrons, the M_1 –A bonds expand and may become completely broken. Indeed, we find that in the negatively charged Cr_2GeC , V_2GeC , Ti_3SnC_2 , V_4AlC_3 , and Cr_2TiAlC_2 , the M_1 –A bond length increases so large that the A atoms are completely detached from the transition metals. As an examples of electron-injected MAX phases, we can consider Li or Na intercalated MAX phases.[99, 100] Our results imply that the electron donated by Li or Na atoms can make the intercalation easier.

In order to understand clearly the effect of charge injection on the structural properties, thicker MAX phases such as Ti_5AlC_4 and Nb_5AlC_4 are preferable than thinner ones. This is because the thinner MAX phases become unstable with only a few electrons injected. Although Ti_5AlC_4 and Nb_5AlC_4 have not been synthesized as phase-pure ternary compounds yet, their solid solutions $(Ti_{0.5}Nb_{0.5})_5AlC_4$ already exist experimentally.[112] Therefore, we examine these two MAX phases Ti_5AlC_4 and Nb_5AlC_4 here. Figure 10 summarizes the results for the bond lengths and the corresponding force constants F_{ij} , as well as the bond strength and the lattice constants, when 1–5 electrons or holes per unit cell are injected into Ti_5AlC_4 . As shown in Fig. 10(a), upon the electron (hole) injection, all bond lengths tend to increase (decrease), and the change of the bond length is larger when the amount of injected charge is larger. It is also clearly observed that the

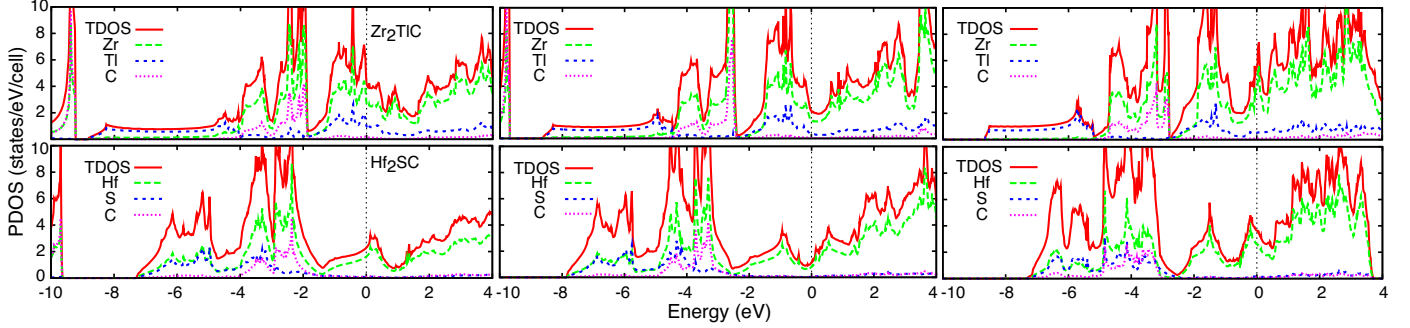


FIG. 9: Projected density of states (PDOS) onto each atomic species (indicated in the figures) for positively, neutral, and negatively charged (from left to right) Zr_2TiC and Hf_2SC (in top and bottom panels). For comparison, the total density of states (TDOS) is also shown. A vertical dotted line at zero energy indicates the Fermi energy.

TABLE V: List of MAX phases sorted in descending order (from top left to bottom right) by the relative bond elongation $\Delta d (= 100 \times \frac{d-d_0}{d_0})$ of the M_1-A bonds after receiving the same amount of electrons per atom. Here, d (d_0) is the M_1-A bond distance in the negatively charged (neutral) MAX phases and only the MAX phases with $\Delta d > 10$ are listed. “Detached” indicates that the A atoms are completely detached from the transition metals upon electron injection. The results for all studied MAX phases are provided in the supporting information file.

V_2GeC (detached)	Cr_2GeC (detached)	Ti_3SnC_2 (detached)
V_4AlC_3 (detached)	Cr_2TiAlC_2 (detached)	Ti_2PbC (20.987)
V_3AlC_2 (18.286)	V_3SiC_2 (16.976)	V_2GaN (16.950)
Sc_2TiC (16.171)	Ti_2TiC (16.155)	Nb_2SC (15.845)
Cr_2GaC (15.515)	Ta_5AlC_4 (15.439)	Cr_2AlC (14.953)
Zr_2TiN (14.729)	Ti_3AuC_2 (14.506)	Nb_5AlC_4 (13.942)
V_2AsC (13.446)	V_2GaC (13.146)	Nb_4AlC_3 (13.099)
Cr_2GaN (12.949)	Ta_4AlC_3 (12.851)	Ti_2InN (12.712)
Hf_2PbC (12.674)	Ti_2SnC (12.601)	Zr_2PbC (12.002)
Nb_2SnC (12.000)	V_2AlC (11.672)	Ti_2SC (11.593)
Ti_4AlN_3 (11.592)	$Mo_2Ti_2AlC_3$ (11.549)	Sc_2InC (11.411)
Mo_2ScAlC_2 (11.153)	Zr_2TiC (11.111)	V_2SiC (10.971)
Hf_2TiC (10.870)	Hf_2SC (10.852)	Nb_2InC (10.650)
V_2PC (10.643)	Ti_2InC (10.311)	Ti_4GeC_3 (10.185)

Ti_1-Al bond is most sensitive to the charge injection. Moreover, as shown in Fig. 10(b), the force constants increases (decreases) with the hole (electron) injection. This occurs because the positive charge injected on either of atoms in the bond would increase the electronegativity and decrease the bond length, resulting in the increase of the ionic contribution to the force constant [$\sim (\chi_X \chi_Y / r^2)^{3/4}$]. Notice also in Fig. 10(b) that after injecting a certain amount of electrons, the force constant of the Ti_1-Al bond becomes very small. This implies that if a larger amount of electrons is injected, the A atom (*i.e.*, Al) becomes detached from the transition metal Ti.

Since the charge injection alters the bond lengths, the

bond strength, *i.e.*, the orbital interaction in the bond, should also be affected. In order to analyze this effect, we also calculate in Fig. 10(c) the ICOHP up to the Fermi energy for the Ti_1-C and Ti_1-Al bonds of Ti_5AlC_4 when electrons or holes are injected. The additional analysis is also provided in the supporting information file. As shown in Fig. 10(c), regardless of the type and amount of the injected charge, the Ti_1-C bonds are always stronger than the Ti_1-Al bonds. Upon the electron (hole) injection, the Ti_1-C and Ti_1-Al bond lengths increase (decrease), and thus their atomic interactions become weaker (stronger). This is consistent with the force constants shown in Fig. 10(b). The analysis of the projected phonon density of states for charged Ti_5AlC_4 also reveals these trends (see the supporting information file). Upon the electron injection, all phonon frequencies decrease and, particularly, the phonon modes projected onto the Al atom become localized at very low phonon frequencies. By injecting a large amount of electrons, the phonon frequencies of the Ti_1-Al bond become almost zero, indicating that the Al atom is almost detached from the Ti atom. It should be noted that the phonon calculations indicate the structural instability of positively charged MAX phases because we find that Ti_5AlC_4 becomes unstable after removing six electrons. This is due to depletion of some of the bonding states. Therefore, upon removing many electrons, the system becomes unstable and might undergo a structural phase transition.

We also investigate in Fig. 10(d) the effect of charge injection on the a and c lattice parameters of Ti_5AlC_4 . As expected, the strongest effect occurs in the c lattice constant because the Ti_1-Al bonds are oriented almost parallel to the c axis. In particular, the electron injection induces large swelling along the c axis in Ti_5AlC_4 and also in other MAX phases in general. This implies that the exfoliation process becomes easier for the negatively charged MAX phases than for the neutral case simply because the M_1-A bonds become longer and weaker upon receiving electrons. The exfoliation of charged MAX phases might be possible experimentally through charge-controlled electrochemical swelling

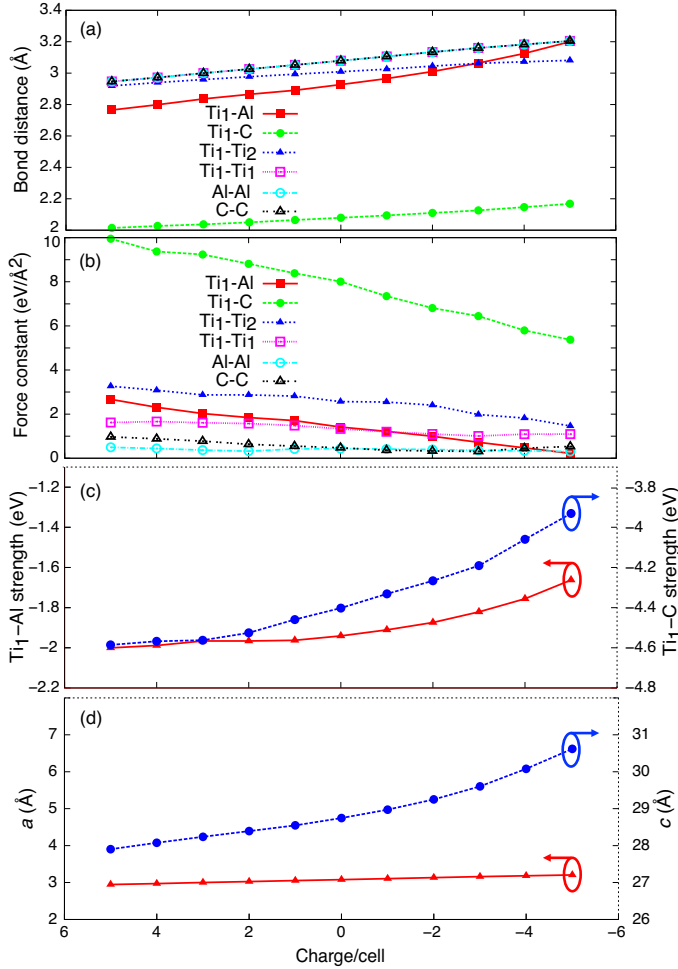


FIG. 10: (a) Bond distances, (b) force constants, (c) bond strength, and (d) lattice parameters of Ti_5AlC_4 when electrons or holes are injected. The horizontal axis represents the number of electrons (negative) or holes (positive) injected per unit cell and zero corresponds to the neutral system.

techniques.[113–123] The volume swelling can also occur using irradiation methods by controlling the density of intrinsic point defects.[124]

Finally, we should note that the atomic position relaxation is essential to correctly capture the trends found above for the charged MAX phases. We have carried out the additional systematic calculations without structural relaxation by using a rigid-band model and the results are shown in the supporting materials files. In particular, we emphasize that the weakening of the bond strength with the electron injection found in Fig. 10(c) would not occur without the atomic position relaxation (as seen in the rigid-band approach), signifying that this is an elastic, not an electronic effect.

We should also remark on the calculations for charged MAX phases. Although the GGA/PBE method can predict the physics of charged MAX phases, the results for the cases of many electrons or holes injected might be biased by the method because the electrons are treated as

being very delocalized. This might be more severe in the case of positively charged MAX phases because one can naively expect that when the transition metals become significantly positively charged after removing a certain number of electrons, the enhanced Coulomb repulsions between the transition metal ions cause the lattice expansion. However, we have observed this expansion in our calculations for negatively charged MAX phases, but not for positively charged ones. This asymmetrical behavior is related to the way that positive and negative charges are distributed in the cell. In both negatively and positively charged cases, there exists a charge neutralizing background and thus the only difference is the extended nature of extra electrons versus the localized nature of extra holes around atomic cores. The repulsion is clearly larger in the case of extended electrons that are closer to each other (on the average) as compared with positive ions, the distance of which is never smaller than the bond lengths. Therefore, we expect that a suitable self-interaction corrected functional would describe the localizations of electrons more accurately. However, in general, we expect a larger repulsion in negatively charged systems than in positively charged ones.

IV. CONCLUSION

MAX phases can be a great source for the synthesis of novel 2D materials with exceptional properties. So far, around 82 different crystalline and numerous alloy MAX phases have been synthesized. Here, we have provided an insight into the exfoliation possibility of various crystalline MAX phases by examining the strength of bonds through force constant calculations, COHP analysis, and the bond order analysis. Our systematic analyses show that in all MAX phases, the $\text{M}_1\text{--X}$ bonds are stiffer and stronger than the $\text{M}_1\text{--A}$ bonds. The large stiffness of the $\text{M}_1\text{--X}$ bonds is attributed to the greater orbital mixing and higher ionicity of the $\text{M}_1\text{--X}$ bonds than those of the $\text{M}_1\text{--A}$ bonds. This is also consistent with the bond order analysis, showing that the $\text{M}_1\text{--X}$ bonds possess higher total number of bonds than the $\text{M}_1\text{--A}$ bonds. The total force constant for the A atoms in MAX phases is found to be linearly correlated with the chemical exfoliation energy, and therefore the force constant can be used to investigate the bond strength and the exfoliation likelihood in MAX phases. The elastic constant C_{33} along the c direction supports this general trend: we have found that C_{33} is also linearly correlated with the exfoliation energy. This implies that the MAX phases with large C_{33} are difficult to be exfoliated into 2D MXenes. This argument for C_{33} is best applied to the M_2AX MAX phases where the number of A layers in the unit cell is comparable with the number of M and X layers.

We have found that except for MAX phases with the A element of S or P, many of the MAX phases are promising candidates for exfoliation into 2D MXenes. Our comprehensive analyses predict that the following MAX phases

have a better chance to be exfoliated successfully into 2D MXenes: Ti_2CdC , Zr_2AlC , Ti_3AuC_2 , Ti_5AlC_4 , Zr_2InC , Hf_2AlC , Ti_2GaC , Ti_4GaC_3 , Hf_2InC , Nb_5AlC_4 , Hf_2TiC , Ti_2InC , Ti_2TiC , Nb_2GaC , Hf_2PbC , Ta_5AlC_4 , Ti_3SiC_2 , Ti_4SiC_3 , Ti_3GeC_2 , Nb_2InC , Ti_2GeC , Ti_4GeC_3 , Hf_2SnC , Mo_2GaC , Ti_2SiC , Ta_2GaC , Cr_2GaN , Ti_3IrC_2 , V_2GaC , Ti_2InN , Ta_2AlC_2 , Ti_2PbC , Ta_2AlC , Cr_2GaC , V_4AlC_3 , V_3AlC_2 , and Ti_2SnC . Therefore, we expect that various 2D MXenes can be synthesized, including Ti_2C , Ti_3C_2 , Ti_4C_3 , Ti_5C_4 , Ti_2N , Zr_2C , Hf_2C , V_2C , V_3C_2 , V_4C_3 , Nb_2C , Nb_5C_4 , Ta_2C , Ta_5C_4 , Cr_2C , Cr_2N , and Mo_2C .

Moreover, we have analyzed the charged MAX phases that exhibit unique electronic properties. Since the states near the Fermi energy are dominated by d orbitals of the transition metals, the injected charges are mainly received by the transition metals. We have shown that the charge injection affects the M_1-A bonds most significantly. Upon receiving electrons, the M_1-A bonds are elongated, and thus the structure is swollen along the c axis, which leads to the decrease of the force constants, thereby facilitating the exfoliation.

Conflicts of interest

There are no conflicts to declare.

Acknowledgements

We are grateful to Dr. Rahul Maitra for fruitful discussion. M.K. and A.R. are also grateful to RIKEN Advanced Center for Computing and Communication (ACCC) for the allocation of computational resource of the RIKEN supercomputer system (HOKUSAI Great-Wave). Part of the calculations were also performed on Numerical Materials Simulator at National Institute for Materials Science (NIMS). M.K. gratefully acknowledges the support by Grant-in-Aid for Scientific Research (No. 17K14804) from MEXT Japan. D.B. and R.D. gratefully acknowledge the IT Center of RWTH Aachen University for providing computational resources and time.

[1] M. W. Barsoum, *Prog. Solid State Chem.*, 2000, **28**, 201–281.

[2] J. Wang and Y. Zhou, *Annu. Rev. Mater. Res.*, 2009, **39**, 415–443.

[3] Z. M. Sun, *Int. Mater. Rev.*, 2011, **56**, 143–166.

[4] D. Horlait, S. C. Middleburgh, A. Chroneos and W. E. Lee, *Sci. Rep.*, 2016, **6**, 18829.

[5] H. Fashandi, M. Dahlqvist, J. Lu, J. Palisaitis, S. I. Simak, I. A. Abrikosov, J. Rosen, L. Hultman, M. Andersson, A. L. Spetz, and P. Eklund, *Nat. Mater.*, 2017, **16**, 814–818.

[6] B. Anasori, M. Dahlqvist, J. Halim, E. J. Moon, J. Lu, B. C. Hosler, E. N. Caspi, S. J. May, L. Hultman, P. Eklund, J. Rosén and M. W. Barsoum, *J. Appl. Phys.*, 2015, **118**, 94304.

[7] R. Meshkian, Q. Tao, M. Dahlqvist, J. Lu, L. Hultman and J. Rosen, *Acta Mater.*, 2017, **125**, 476–480.

[8] Q. Tao, M. Dahlqvist, J. Lu, S. Kota, R. Meshkian, J. Halim, J. Palisaitis, L. Hultman, M. W. Barsoum, P. O. Persson and J. Rosen, *Nat. Commun.*, 2017, **8**, 14949.

[9] M. Dahlqvist, J. Lu, R. Meshkian, Q. Tao, L. Hultman and J. Rosen, *Sci. Adv.*, 2017, **3**, e1700642.

[10] M. F. Cover, O. Warschkow, M. M. M. Bilek and D. R. McKenzie, *J. Phys.: Condens. Matter*, 2009, **21**, 305403.

[11] M. Dahlqvist, B. Alling and J. Rosén, *Phys. Rev. B*, 2010, **81**, 220102(R).

[12] Y. Mo, P. Rulis and W. Y. Ching, *Phys. Rev. B*, 2012, **86**, 165122.

[13] M. Khazaei, M. Arai, T. Sasaki, M. Estili and Y. Sakka, *J. Phys.: Condens. Matter*, 2014, **26**, 505503.

[14] M. Khazaei, M. Arai, T. Sasaki, M. Estili and Y. Sakka, *Sci. Tech. Adv. Mater.*, 2014, **15**, 014208.

[15] S. Aryal, R. Sakidja, M. W. Barsoum and W. -Y. Ching, *Phys. Status Solidi B*, 2014, **251**, 1480–1497.

[16] M. Dahlqvist and J. Rosén, *Phys. Chem. Chem. Phys.*, 2015, **17**, 31810.

[17] M. Ashton, R. G. Hennig, S. R. Broderick, K. Rajan and S. B. Sinnott, *Phys. Rev. B*, 2016, **94**, 054116.

[18] A. Talapatra, T. Duong, W. Son, H. Gao, M. Radovic and R. Arróyave, *Phys. Rev. B*, 2016, **94**, 104106.

[19] R. Arróyave, A. Talapatra, T. Duong, W. Son, H. Gao and M. Radovic, *Mater. Res. Lett.*, 2017, **5**, 170–178.

[20] C. Jiang and A. Chroneos, *Phys. Chem. Chem. Phys.*, 2017, DOI:10.1039/c7cp07576f.

[21] Z. Sun, D. Music, R. Ahuja and J. M. Schneider, *J. Phys. Condens. Matter*, 2005, **17**, L15.

[22] M. A. Ghebouli, B. Ghebouli, A. Bouhemadou and M. Fatmi, *Solid State Commun.*, 2011, **151**, 382–387.

[23] M. T. Nasir, M. A. Hadi, S. H. Naqib, F. Parvin, A. K. M. A. Islam, M. Roknuzzaman and M. S. Ali, *Int. J. Mod. Phys. B*, 2014, **28**, 1550022.

[24] M. A. Hadi and M. S. Ali, *Chin. Phys. B*, 2016, **25**, 107103.

[25] M. A. Hadi, S. H. Naqib, S. -R. G. Christopoulos, A. Chroneos and A. K. M. A. Islam, *J. Alloys Compd.*, 2017, **724**, 1167.

[26] Z. Sun, S. Li, R. Ahuja and J. M. Schneider, *Solid State Commun.*, 2004, **129**, 589–592.

[27] J. D. Hettinger, S. E. Lofland, P. Finkel, T. Meehan, J. Palma, K. Harrell, S. Gupta, A. Ganguly, T. El-Raghy and M. W. Barsoum, *Phys. Rev. B*, 2005, **72**, 115120.

[28] M. Naguib, M. Kurtoglu, V. Presser, J. Lu, J. Niu, M. Heon, L. Hultman, Y. Gogotsi and M. W. Barsoum, *Adv. Mater.*, 2011, **23**, 4248–4253.

[29] M. Naguib, O. Mashtalir, J. Carle, V. Presser, J. Lu, L. Hultman, Y. Gogotsi and M. W. Barsoum, *ACS Nano*, 2012, **6**, 1322–1331.

[30] B. Soundiraraju and B. K. George, *ACS Nano*, 2017, **11**, 8892–8900.

[31] M. Naguib, J. Halim, J. Lu, K. M. Cook, L. Hultman, Y. Gogotsi and M. W. Barsoum, *J. Am. Chem. Soc.*, 2013, **135**, 15966–15969.

[32] R. Meshkini, L. -Å. Näslund and J. Halim, *Scr. Mater.*,

2015, **108**, 147–150.

[33] J. Zhou, X. Zha, F. Y. Chen, Q. Ye, P. Eklund, S. Du and Q. Huang, *Angew. Chem.-Int. Edit.*, 2016, **55**, 5008.

[34] M. Ghidiu, M. Naguib, C. Shi, O. Mashtalir, L. M. Pan, B. Zhang, J. Yang, Y. Gogotsi, S. J. L. Billinge and M. W. Barsoum, *Chem. Commun.*, 2014, **50**, 9517.

[35] J. Yang, M. Naguib, M. Ghidiu, L. -M. Pan, J. Gu, J. Nanda, J. Halim, Y. Gogotsi and M. W. Barsoum, *J. Am. Ceramic Soc.*, 2016, **99**, 660.

[36] P. Urbankowski, B. Anasori, T. Makaryan, D. Er, S. Kota, P. L. Walsh, M. Zhao, V. B. Shenoy, M. W. Barsoum and Y. Gogotsi, *Nanoscale*, 2016, **8**, 11385.

[37] B. Anasori, Y. Xie, M. Beidaghi, J. Lu, B. C. Hosler, L. Hultman, P. R. C. Kent, Y. Gogotsi and M. W. Barsoum, *ACS Nano*, 2015, **9**, 9507–9516.

[38] M. Khazaei, M. Arai, T. Sasaki, C. -Y. Chung, N. S. Venkataraman, M. Estili, Y. Sakka and Y. Kawazoe, *Adv. Funct. Mater.*, 2013, **23**, 2185–2192.

[39] M. Khazaei, M. Arai, T. Sasaki, M. Estili and Y. Sakka, *Phys. Chem. Chem. Phys.*, 2014, **16**, 7841–7849.

[40] M. Khazaei, M. Arai, T. Sasaki, A. Ranjbar, Y. Liang and S. Yunoki, *Phys. Rev. B*, 2015, **92**, 075411.

[41] H. Weng, A. Ranjbar, Y. Liang, Z. Song, M. Khazaei, S. Yunoki, M. Arai, Y. Kawazoe, Z. Fang and X. Dai, *Phys. Rev. B*, 2015, **92**, 075436.

[42] M. Khazaei, A. Ranjbar, M. Ghorbani-Asl, M. Arai, T. Sasaki, Y. Liang and S. Yunoki, *Phys. Rev. B*, 2016, **93**, 205125.

[43] M. Khazaei, A. Ranjbar, M. Arai and S. Yunoki, *Phys. Rev. B*, 2016, **94**, 125152.

[44] Y. Liang, M. Khazaei, A. Ranjbar, M. Arai, S. Yunoki, Y. Kawazoe, H. Weng, and Z. Fang, Theoretical prediction of two-dimensional functionalized MXene nitrides as topological insulators, *Phys. Rev. B*, 2017, **96**, 195414.

[45] H. Lashgari, M. R. Abolhassani, A. Boochani, S. M. Elahi and J. Khodadadi, *Solid State Commun.*, 2014, **195**, 61–69.

[46] Z. Guo, J. Zhou, C. Si and Z. Sun, *Phys. Chem. Chem. Phys.*, 2015, **17**, 15348.

[47] C. Si, J. Zhou and Z. Sun, *ACS Appl. Mater. Interfaces*, 2015, **7**, 17510–17515.

[48] J. He, P. Lyu, L. Z. Sun, Á. M. García and P. Nachtigall, *J. Mater. Chem. C*, 2016, **4**, 6500–6509.

[49] M. Je, Y. Lee and Y. -C. Chung, *Thin Solid Films* 2016, **619**, 131–136.

[50] G. Gao, G. Ding, J. Li, K. Yao, M. Wu and M. Qian, *Nanoscale*, 2016, **8**, 8986–8994.

[51] H. Kumar, N. C. Frey, L. Dong, B. Anasori, Y. Gogotsi and V. B. Shenoy, *ACS Nano*, 2017, **11**, 7648–7655.

[52] Z. Guo, J. Zhou, L. Zhu, Z. Sun, *J. Mater. Chem. A*, 2016, **4**, 11446–11452.

[53] Y. Lee, Y. Hwang and Y. C. Chung, *ACS Appl. Mater. Interfaces*, 2015, **7**, 7163–7169.

[54] X. -F. Yu, Y. Li, J. -B. Cheng, Z. -B. Liu, Q. -Z. Li, W. -Z. Li, X. Yang and B. Xiao, *ACS Appl. Mater. Interfaces*, 2015, **7**, 13707–13713.

[55] S. Lai, J. Jeong, S. K. Jang, J. Xu, Y. J. Choi, J. -H. Park, E. Hwang and S. Lee, *Nanoscale*, 2015, **7**, 19390–19396.

[56] F. Shahzad, M. Alhabeb, C. B. Hatter, B. Anasori, S. M. Hong, C. M. Koo and Y. Gogotsi, *Science*, 2016, **353**, 1137–1140.

[57] Y. Yang, S. Umrao, S. Lai and S. Lee, *J. Phys. Chem. Lett.*, 2017, **8**, 859–865.

[58] Y. Xie, Y. Dall’Agnese, M. Naguib, Y. Gogotsi, M. W. Barsoum, H. L. Zhuang and P. R. C. Kent, *ACS Nano*, 2014, **8**, 9606–9615.

[59] R. B. Rakhi, B. Ahmed, M. N. Hedhili, D. H. Anjum and H. N. Alshareef, *Chem. Mater.*, 2015, **27**, 5314–5323.

[60] H. Kim, B. Anasori, Y. Gogotsi and H. N. Alshareef, *Chem. Mater.*, 2017, **29**, 6472–6479.

[61] H. Lin, X. Wang, L. Yu, Y. Chen and J. Shi, *Nano Lett.*, 2017, **17**, 384–391.

[62] G. Fan, X. Li, Y. Ma, Y. Zhang, J. Wu, B. Xu, T. Sun, D. Gao and J. Bi, *New J. Chem.*, 2017, **41**, 2793–2799.

[63] J. Ran, G. Gao, F. -T. Li, T. -Y. Ma, A. Du, S. -Z. Qiao, *Nat. Commun.*, 2017, **8**, 13907.

[64] X. Zhang, J. Xu, H. Wang, J. Zhang, H. Yan, B. Pan, J. Zhou and Y. Xie, *Angew. Chem. Int. Ed. Engl.*, 2013, **52**, 4361.

[65] M. Xue, Z. Wang, F. Yuan, X. Zhang, W. Wei, H. Tang and C. Li, *RSC Adv.*, 2017, **7**, 4312–4319.

[66] B. Anasori, M. R. Lukatskaya and Y. Gogotsi, *Nat. Rev.*, 2017, **1**, 16098.

[67] M. Khazaei, A. Ranjbar, M. Arai, T. Sasaki and S. Yunoki, *J. Mater. Chem. C*, 2017, **5**, 2488–2503.

[68] Z. Guo, L. Zhu, J. Zhou and Z. Sun, *RSC Adv.*, 2015, **5**, 25403–25408.

[69] G. Kresse and J. Furthmüller, *Comput. Mater. Sci.*, 1996, **6**, 15–50.

[70] J. P. Perdew, K. Burke and M. Ernzerhof, *Phys. Rev. Lett.*, 1996, **77**, 3865.

[71] H. J. Monkhorst and J. D. Pack, *Phys. Rev. B*, 1976, **13**, 5188.

[72] A. Togo, F. Oba and I. Tanaka, *Phys. Rev. B*, 2008, **78**, 134106.

[73] A. J. E. Foreman and W. M. Lomer, *Proc. Phys. Soc. London, Sect. B*, 1957, **70**, 1143.

[74] Y. Liu, K. T. E. Chua, T. C. Sum, C. K. Gan, *Phys. Chem. Chem. Phys.*, 2014, **16**, 345–350.

[75] R. Dronskowski and P. E. Blöchl, *J. Phys. Chem.*, 1993, **97**, 8617–8624.

[76] M. Küpers, P. M. Konze, S. Maintz, S. Steinberg and A. M. Mio, Cojocaru-Miredin, O.; Zhu, M.; Müller, M.; Luysberg, M.; Mayer, J.; Wuttig, M.; Dronskowski, R. *Angew. Chem. Int. Ed.*, 2017, **56**, 10204–1028.

[77] V. L. Deringer, A. L. Tchougréeff and R. Dronskowski, *J. Phys. Chem. A*, 2011, **115**, 5461–5466.

[78] S. Maintz, V. L. Deringer, A. L. Tchougréeff, R. Dronskowski, *J. Comput. Chem.*, 2013, **34**, 2557–2567.

[79] S. Maintz, V. L. Deringer, A. L. Tchougréeff and R. Dronskowski, *J. Comput. Chem.*, 2016, **37**, 1030–1035.

[80] L. Pauling, *J. Am. Chem. Soc.*, 1947, **69**, 542–553.

[81] L. Pauling and B. Kamb, *Proc. Natl. Acad. Sci. USA*, 1986, **83**, 3569.

[82] V. L. Deringer, R. P. Stoffel, M. Wuttig and R. Dronskowski, *Chem. Sci.*, 2015, **6**, 5255–5262.

[83] N. W. Tideswell, F. H. Kruse and J. D. McCullough, *Acta Cryst.*, 1957, **10**, 99–102.

[84] P. Pyykkö and M. Atsumi, *Chem. Eur. J.*, 2009, **15**, 186–197.

[85] L. Fast, J. M. Wills, B. Johansson and O. Eriksson, *Phys. Rev. B*, 1995, **51**, 17431–17438.

[86] P. Srivastava, A. Mishra, H. Mizuseki, K. -R. Lee and A. K. Singh, *ACS Appl. Mater. Interfaces*, 2016, **8**, 24256–24264.

[87] A. Mishra, P. Srivastava, H. Mizuseki, K. -R. Lee and A. K. Singh, *Phys. Chem. Chem. Phys.*, 2016, **18**, 11073–11080.

[88] R. G. Pearson, *J. Molecular. Struc.*, 1993, **300**, 519–525.

[89] K. Brandhorst and J. Grunenberg, *Chem. Soc. Rev.*, 2008, **37**, 1558–1567.

[90] D. Cremer and E. Kraka, *Curr. Org. Chem.*, 2010, **14**, 1524–1560.

[91] J. R. Lombardi and B. Davis, *Chem. Rev.*, 2002, **102**, 2431–2460.

[92] H. -B. Bürgi and J. D. Dunitz, *J. Am. Chem. Soc.*, 1987, **109**, 2924–2926.

[93] H. S. Johnston, *J. Am. Chem. Soc.*, 1964, **86**, 1643.

[94] J. Hong and O. Delaire, *arXive: 1604.07077v2 [cond-mat.mtrl-sci]*, 2016.

[95] O. V. Pupysheva, A. A. Farajian, C. R. Knick, A. Zhamu and B. Z. Jang, *J. Phys. Chem. C*, 2010, **114**, 21083–21087.

[96] L. Wang, X. Zhou, T. Ma, D. Liu, L. Gao, X. Li, J. Zhang, Y. Hu, H. Wang, Y. Dai and J. Luo, *Nanoscale*, 2017, **9**, 10846–10853.

[97] Z. Sun, D. Music, R. Ahuja, S. Li and J. M. Schneider, *Phys. Rev. B*, 2004, **70**, 092102.

[98] D. Music, Z. Sun, R. Ahuja, S. Li and J. M. Schneider, Coupling in nanolaminated ternary carbides studied by theoretical means: the influence of electronic potential applications, *Phys. Rev. B*, 2006, **73**, 134117.

[99] J. Xu, M. -Q. Zhao, Y. Wang, W. Yao, C. Chen, B. Anasori, A. Sarycheva, C. E. Ren, T. Mathis, L. Gomes, L. Zhenghua and Y. Gogotsi, *ACS Energy Lett.*, 2016, **1**, 1094–1099.

[100] A. T. Tesfaye, Y. Gogotsi and T. Djenizian, *Electrochem. Commun.*, 2017, **81**, 29–33.

[101] D. Cremer, A. Wu, A. Larsson and E. Kraka, *J. Mol. Model.* **2000**, **6**, 396–412.

[102] R. Dronskowski, Computational Chemistry of Solid State Materials, Wiley-VCH, Weinheim, New York, 2005.

[103] D. Music, A. Houben, R. Dronskowski and J. M. Schneider, *Phys. Rev. B*, 2007, **75**, 174102.

[104] M. Esser, S. Maintz and R. Dronskowski, *J. Comput. Chem.*, 2017, **38**, 620–628.

[105] W. Gordy, *J. Chem. Phys.*, 1946, **14**, 305–320.

[106] W. Gordy and J. O. Thomas, *J. Chem. Phys.*, 1956, **24**, 439–444.

[107] S. Kaya, C. Kaya, I. B. Obot and N. Islam, *Spectrochim. Acta Mol. Biomol. Spectrosc.*, 2016, **154**, 103–107 (2016).

[108] A. L. Allred and E. G. Rochow, *J. Inorg. Nucl. Chem.*, 1958, **5**, 264–268.

[109] G. Henkelman, A. Arnaldsson and H. Jónsson, *Comput. Mater. Sci.*, 2006, **36**, 354–360.

[110] E. Sanville, S. D. Kenny, R. Smith and G. Henkelman, *J. Comp. Chem.*, 2007, **28**, 899–908.

[111] W. Tang, E. Sanville and G. Henkelman, *J. Phys.: Compute Mater.*, 2009, **21**, 084204.

[112] L. Zheng, J. Wang, X. Lu, F. Li, J. Wang and Y. Zhou, *J. Am. Ceram. Soc.*, 2010, **93**, 3068–3071.

[113] H. Suquet, J. T. Iiyama, H. Kodama, H. Pezerat, *Clays and Clay Minerals*, 1977, **25**, 231–242.

[114] A. Fitch, J. Du, H. Gan and J. W. Stucki, *Clays and Clay Minerals*, 1995, **43**, 607–614.

[115] K. K. Mohan and H. S. Fogler, *Langmuir*, 1997, **13**, 2863–2872.

[116] A. Fernández-Nieves, A. Fernández-Barbero, B. Vincent and F. J. de las Neives, *Macromolecules*, 2000, **33**, 2114–2118.

[117] J. -C. P. Gabriel, F. Camerel, B. J. Lemaire, H. Desvaux, P. Davidson and P. Batail, *Nature*, 2001, **413**, 504–508.

[118] D. A. Laird, *Appl. Clay Sci.*, 2006, **34**, 74–87.

[119] F. Kaasik, T. Tamm, M. M. Hantel, E. Perre, A. Aabloo, E. Lust, M. Z. Bazant and V. Presser, *Electrochem. Commun.*, 2013, **34**, 196–199.

[120] J. K. Riley, K. Matyjaszewski and R. D. Tilton, *Langmuir*, 2014, **30**, 4056–4065.

[121] R. Zahn, J. Vörös and T. Zambelli, *Langmuir*, 2014, **30**, 12057–12066.

[122] S. Rosenfeldt, M. Stöter, M. Schlenk, T. Martin, R. Q. Albuquerque, S. Förster and J. Breu, *Langmuir*, 2016, **32**, 10582–10588.

[123] M. C. Pazos, M. A. Castro, A. Cota, F. J. Osuna, E. Pavón and M. D. Alba, *J. Ind. Eng. Chem.*, 2017, **52**, 179–186.

[124] J. M. Pruneda, T. D. Archer and E. Artacho, *Phys. Rev. B*, 2004, **70**, 104111.